International Journal of Computational Fluid Dynamics

ISSN: 1061-8562 (Print) 1029-0257 (Online) Journal homepage: http://www.tandfonline.com/loi/gcfd20

# ISPH modelling of transient natural convection

M. E. Danis , M. Orhan & A. Ecder

**To cite this article:** M. E. Danis , M. Orhan & A. Ecder (2013) ISPH modelling of transient natural convection, International Journal of Computational Fluid Dynamics, 27:1, 15-31, DOI: 10.1080/10618562.2012.753146

**To link to this article:** http://dx.doi.org/10.1080/10618562.2012.753146

*International Journal of Computational Fluid Dynamics*, 2013
Vol. 27, No. 1, 15–31, http://dx.doi.org/10.1080/10618562.2012.753146

Taylor & Francis
Taylor & Francis Group

# ISPH modelling of transient natural convection

M.E. Danış[a,*], M. Orhan[b] and A. Ecder[a]

[a]*Department of Mechanical Engineering, Bogazici University, Bebek, Istanbul, Turkey;* [b]*Department of Mechanical Engineering, Pamukkale University, Kinikli, Denizli, Turkey*

(*Received 2 August 2012; final version received 16 November 2012*)

Transient and laminar natural convection in a square cavity has been investigated using smoothed particle hydrodynamics (SPH) technique as a discretisation tool on uniform Eulerian grids. Although SPH is a mesh-free Lagrangian method and always applied to discretise the Lagrangian form of governing equations, in this study Eulerian form is discretised using SPH operators. This approach is thought to be the upper limit of accuracy of Lagrangian SPH computations by preventing density error accumulation and particle disordering. In the present method, incompressibility is strictly enforced by employing SPH pressure projection method in order to obtain a divergence-free velocity field as in the incompressible SPH (ISPH) method. Natural convection in a square cavity is simulated for Rayleigh numbers, $Ra$, between $10^3$ and $10^6$. The effect of $Ra$ on the flow field and heat transfer characteristics is investigated and the method is validated by data available in the literature. Results obtained from ISPH method on Eulerian grids are in excellent agreement with data available in the literature.

**Keywords:** incompressible smoothed particle hydrodynamics; natural convection; pressure projection; meshless methods; cavity flow

## 1. Introduction

Modelling of natural convection is essential not only for the better understanding of heat transfer phenomena, but also for the development and selection of materials, motivating achievement in solidification and crystal growth research (e.g. Giangi and Stella 1999; Lappa 2004; Kohno and Tanahashi 2005). Other applications include cooling of electronics equipment, re-circulating flow driven by temperature and salinity differences, pollution, flows generated by fires, etc. (e.g. Kuznetsov and Sitnikova 2004; Ilicak, Ecder, and Turan 2007; Teamah, Dawood, and El-Maghlany 2011; Nelson, Butler, and Weise 2012). Hence, studies investigating the physics of natural convection and aiming at accurate solutions of them are still in demand.

Smoothed particle hydrodynamics (SPH) was originally invented by Lucy (1977) and Gingold and Monaghan (1977) as a truly meshless Lagrangian method in order to simulate astrophysical problems. Although it was invented to solve astrophysical problems, SPH now has a wide range of applications in fluid mechanics, solid mechanics, high velocity impact problems, and the film and computer games industry.

In SPH, a continuum is modelled by a finite set of particles that can freely move in a computational domain. These particles are not physical particles. Instead, SPH particles are hypothetical particles and they may be thought of as moving versions of fixed Eulerian grid nodes but obeying the Lagrangian form of governing equations. Since particles can change their position in a certain time period, they do not have geometrically fixed relations with each other. For instance, an interaction between any two particles may change at a later time step and even may not exist anymore. Thus, fixed discretisation schemes in grid-based methods, e.g. finite difference, cannot be used in meshless methods. To model and discretise a continuum, the particle interactions are defined by smoothing kernels (smoothing functions or weighting functions) in SPH (Liu and Liu 2003). In the neighbourhood of a specified particle, the smoothing kernels are used to calculate how much effect neighbouring particles have on this specified particle. Thus, in a typical SPH time step, a neighbour list for each particle must be constructed and smoothing kernels and their derivatives must be calculated immediately after particles are moved. All mathematical operators in governing equations, e.g. derivative, gradient, divergence and Laplacian operators, are discretised and calculated according to a neighbour list, smoothing kernel and derivatives of the smoothing kernel. For a field variable, e.g. position, velocity, temperature and density, inserting the obtained values of mathematical operators into governing equations, material time rate of change is calculated and particles are moved. At the new position, new values for field variables are obtained by implementing a proper numerical integration scheme. This process is repeated until a steady state is reached.

*Corresponding author. Email: engin.danis@boun.edu.tr

First incompressible flow simulation using SPH was performed by Monaghan (1994) in which free surface flows, such as elliptical drop, bursting dam, bore and wavemaker problems, were studied. One of the most interesting features of this work is that incompressibility was approximated by weakly compressible (WC) approach. This is based on the observation that density variation is proportional to the square of Mach number, $Ma^2$. However, the speed of sound in an incompressible fluid is very large and Mach number is very small. Therefore, incompressible fluid is approximated with an artificial fluid in which speed of sound is decreased and Mach number is increased. It is worth noting that Mach number is still small enough to approximate an incompressible fluid. In the SPH literature, Mach number is usually chosen between $10^{-1}$ and $10^{-2}$. Thus, density variation changes from $10^{-2}$ to $10^{-4}$, which means that flow is nearly incompressible. Another interesting feature of this work is that pressure was treated as a function of density and calculated from an equation of state. This approach is known as Weakly Compressible SPH (WCSPH) and today, it is one of the most popular SPH approaches for incompressible flow simulations.

Another incompressible approach was presented by Morris, Fox, and Zhu (1997) in which low Reynolds number problems, such as Couette flow, Poiseuille flow and flow past a cylinder, were simulated. As opposed to the equation of state used by Monaghan (1994), Morris, Fox, and Zhu (1997) used a different equation of state. Furthermore, in order to model solid boundaries, Morris, Fox, and Zhu (1997) introduced mirror particle method for the first time in SPH simulations. This is another difference from the work of Monaghan (1994), where a repulsive force is used in order to model solid boundaries, which is very similar to Lennard-Jones force in molecular dynamics (MD) simulations.

However, classical WCSPH approach has some limitations and weaknesses. For instance, it is not able to simulate moderate or high Reynolds number flows accurately. Therefore, instead of the classical WCSPH approach, advanced approaches are implemented to WCSPH. Using proper turbulence models, WCSPH is able to simulate high Reynolds number flows (Gomez-Gesteira et al. 2012; Shao et al. 2012). Moreover, increasing speed of sound decreases time increment limit due to Courant-Friedrichs-Lewy (CFL) condition. Therefore, computational time and effort spent to reach steady state is increased. In addition to these, pressure field is very sensitive to density fluctuations since pressure is calculated as function of density using an equation of state in WCSPH. Therefore, fluctuations in density field result in oscillations in pressure field. Hence, several approaches are introduced in order to reduce density fluctuations and resulting oscillations in pressure field.

One of these approaches is called Incompressible SPH (ISPH). In ISPH method, incompressibility is directly enforced and an intermediate velocity field is obtained without considering gradient of pressure. The intermediate velocity field is, then, projected onto a divergence-free velocity space, which results in a pressure Poisson equation (PPE). After solving PPE, intermediate velocity field is corrected to obtain a new velocity field, which is divergence-free. This method is based on Helmholtz–Hodge decomposition and it was first introduced to SPH context by Cummins and Rudman (1999). In their study, this projection approach was termed PSPH but nowadays, it is usually called Divergence-Free Incompressible SPH (ISPH-DF).

Similar to the SPH projection method presented by Cummins and Rudman (1999), Shao and Lo (2003) suggested another SPH projection approach that enforces incompressibility by using density invariance. In their method, an intermediate velocity field is calculated without considering the gradient of pressure as in Cummins and Rudman (1999). At this stage, instead of projecting the intermediate velocity field onto a divergence-free velocity field, density variation is projected. By this way, accumulation of density errors in divergence-free ISPH is not observed. This approach is called Density Invariant Incompressible SPH (ISPH-DI). They used their approach for simulations of near-shore solitary wave mechanics with a large eddy simulation.

Another projection-based ISPH method was introduced by Pozorski and Wawrenczuk (2002). A procedure similar to the one that was presented by Cummins and Rudman (1999) was followed. At the end of each time step, an additional PPE is solved in order to obtain a constant density field and particle positions are updated due to the resulting pressure gradient. They tested their algorithm for one-dimensional viscous damping, Couette and Poiseuille flows, lid-driven cavity flows and Rayleigh–Taylor instability flows.

Furthermore, Colin, Egli, and Lin (2006) proposed a pure SPH solution of Helmholtz decomposition in order to obtain a null divergence field. Moreover, a new version of Laplacian operator was introduced. In addition to these, different SPH gradient operators were compared. They concluded that difference gradient approximation formula gives better results and is more compatible with the new Laplacian operator.

Moreover, Hu and Adams (2007) suggested an approach similar to Pozorski and Wawrenczuk (2002) by combining ISPH-DF and ISPH-DI in order to simulate multiphase incompressible flows. This method is known as Divergence-Free and Density Invariant Incompressible SPH (ISPH-DFDI). In this approach, first of all, density invariant approach is used as internal iterations until density variation is lower than a desired tolerance. In other words, density projected PPE is solved and particle positions are updated repeatedly until uniform particle distribution is obtained. After the internal iterations are completed, divergence-free approach is used in order to obtain a divergence-free velocity field. In the best case, two PPE are solved in each time step and if a uniform particle distribution is not obtained at

the first internal iteration, the number of internal PPEs to be solved is increased. Although this increases computational cost, this approach results in uniform particle distribution and thus increased accuracy.

In addition to these, Xu, Stansby, and Laurence (2009) introduced a particle shifting method that prevents anisotropic particle distribution resulting in ISPH methods together with an extensive comparison of ISPH-DF, ISPH-DI and ISPH-DFDI. According to Xu, Stansby, and Laurence (2009), hydrodynamic variables are corrected using a Taylor series expansion and more isotropic particle distributions are obtained. Although the particle shifting method is not a strictly conservative method, it increases accuracy of simulations. This approach is called *Divergence-Free Incompressible SPH with shifting particle position* (ISPH-DFS). In the study of Xu, Stansby, and Laurence (2009), accuracy tests were performed for Taylor–Green vortices and vortex spin-down problems. Moreover, ISPH-DFS method was validated with benchmark problems lid-driven cavity and two-dimensional (2-D) laminar flow past a circular cylinder. Free surface flows, e.g. impulsive paddle and 2-D dam break, were investigated using ISPH-DFS method.

Szewc, Pozorski, and Minier (2012) investigated the incompressibility constraint in SPH. They analysed WC-SPH, grid projected ISPH and particle projected ISPH for the same kind of boundary conditions for a direct comparison of these approaches. They pointed out accumulation of density error in ISPH simulation. To prevent accumulation of density errors, they made use of the ISPH algorithm proposed by Pozorski and Wawrenczuk (2002). However, they suggested to include second PPE if density variation exceeds a certain threshold value. Therefore, they reduced computational cost as well as density variation.

A different approach for solving PPE was presented by Hosseini, Manzari, and Hannani (2007). They proposed a three-step explicit algorithm for simulation of non-Newtonian fluid flow in which PPE was solved explicitly. In their work, Hosseini, Manzari, and Hannani (2007) only included body force terms in the first step. In the second step, viscous terms were included and density variation was projected onto a divergence-free velocity field. After solving PPE explicitly, velocity field and particle positions were corrected in the third step.

In general, projection-based ISPH approaches make use of an iterative method in order to solve PPE implicitly. In the SPH literature, the most common solvers are conjugate gradient (CG) and bi-conjugate gradient stabilised (BiCGSTAB) methods. Especially, BiCGSTAB is preferred since it smooths out the residual and enhances the convergence according to van der Vorst (1992).

Apart from the projection-based ISPH methodologies, Ellero, Serrano, and Espanol (2007) presented a different ISPH approach. They used Lagrange multipliers in order to enforce incompressibility and set constant volume of the fluid particles as their kinematic constraint. Then, they solved the constraint equation using the SHAKE methodology in order to obtain Lagrange multipliers, which are the non-thermodynamics pressure values resulting from kinematic restrictions.

The usage of SPH in incompressible flow simulations is not limited to isothermal case. Chaniotis, Poulikakos, and Koumoutsakos (2002) proposed a remeshing algorithm using WC approach and performed a comprehensive study for non-isothermal flows. Remeshing procedure was tested for some benchmark problems of flow and energy transport such as one-dimensional shock-tube problem, two-dimensional Taylor–Green flow, 2-D double shear layer, lid-driven flow in a square cavity, natural convection in a differentially heated cavity and mixed convection in a driven cavity. Results showed that remeshing improved the accuracy of simulations since uniform particle spacing was conserved in each time step. Moreover, Chaniotis, Poulikakos, and Koumoutsakos (2002) used remeshing procedure in the study of effect of jet pulsation on heat transfer and flow characteristics of single and double jet impingement on a heated surface, simulation of laminar chemically reacting and interfacial flows.

Another simulation of flow and energy transport using SPH was performed by Szewc, Pozorski, and Tanière (2011). Natural convection in a square cavity problem with a Boussinesq and a non-Boussinesq formulation was studied. They performed simulations at $Ra = 10^3$, $Ra = 10^4$ and $Ra = 10^5$ with $Pr = 0.71$. They investigated the effect of Gay-Lussac number on velocity field and Nusselt number for non-Boussinesq formulation. They reported that their results were in good agreement with other numerical experiments. Since they used WC approach, velocity and temperature fields showed oscillations.

Although SPH achieves a great success in simulating fluid flow accurately, there are still certain limitations due to the mesh-free character of the method. One of these limitations is the tensile instability problem, which results in clustering of particles (Monaghan 2000). Since a uniform distribution of particles is necessary for incompressible flow simulations, there were attempts to solve the tensile instability problem by introducing artificial pressure (Monaghan 2000), projection methods (Cummins and Rudman 1999; Shao and Lo 2003; Hu and Adams 2007) and particle shifting techniques (Xu, Stansby, and Laurence 2009).

Despite the fact that higher accuracy can be achieved, quantification of errors due to Lagrangian artifacts, such as particle clustering, is still an important issue. There are some techniques predicting numerical and modelling errors such as reported in Roache (1997), Oden and Vemaganti (2000), Afshar and Shobeyri (2010) and many others. Employment of method of a-posteriori error approximation for prediction of errors induced by particle clustering seems to be possible. For this purpose, SPH discretisation can be introduced to the weak formulation of Navier–Stokes

equations. Then, an error equation for each flow variable can be constructed. At this stage, the difference between the evenly distributed and clustered particles should come into effect in error equation by introduction of a parameter. In our opinion, a comparison between the radial distribution functions of each system is a very good candidate for determining the mentioned parameter. It should be noted that the task of measuring errors itself is a very complicated task (Prudhomme and Oden 2002). However, instead of this, the bounds of error can be identified theoretically by the use of residual functionals (Prudhomme and Oden 1999). The amount of error between evenly distributed and disordered particles can be quantified by an energy norm, such as given in Ciarlet (1978).

In the present study, as opposed to conventional SPH approaches, SPH particles are kept stationary. The aim here is to test the upper limit of accuracy of SPH computations. Since all particles are stationary, the Eulerian form of governing equations is used instead of the Lagrangian form of governing equations. ISPH method is used to simulate transient and laminar natural convection in a square cavity with Boussinesq approximation. For solid boundary modelling, mirror particle approach in Morris, Fox, and Zhu (1997) is implemented.

The most important advantage of this approach is that density field is kept constant and uniformity of particle distribution is guaranteed during simulations. In other words, the approach presented here prevents density error accumulation and particle disorder, which are reported as limiting factors of the capacity of ISPH method. Since constant density field and uniform particle distribution increase the accuracy of kernel approximations, this approach can be deduced to be the upper limit of SPH computations.

However, the approach proposed in this paper naturally loses some advantages of Lagrangian SPH. For instance, Lagrangian applications of SPH in multiphase flows do not require any additional process to model interfaces. By its nature, Lagrangian SPH handles interfaces automatically. On the other hand, many Eulerian methods (e.g. PIC, MAC, VOF, Level set method, etc.) can model multiphase flows (Ren et al. 2011) but these methods introduce either additional equations or models. Similarly, our approach requires such an additional tool to model interface. However, the goal of this study is to test the upper limit of accuracy of SPH simulation. Therefore, our approach mainly focuses on preventing fundamental causes of errors in the Lagrangian SPH simulation (density error and particle disorder) rather than proposing a general approach of application although this is possible as in many Eulerian methods.

This paper is arranged in the following way. In Section 2, mathematical modelling of natural convection is discussed. Geometry of computational domain is described and governing equations of transient and laminar natural convection are presented. Non-dimensionalisation of governing equations are also presented. In Section 3, SPH methodology is discussed. Derivation of SPH summation formula is made and SPH forms of mathematical operators (derivative, gradient, divergence and Laplacian operators) are given. Moreover, apart from the conventional operators, frequently used high-order SPH approximation schemes and their effect in grid-based ISPH method are discussed in detail. In Section 4, ISPH formulation of governing equations are given. Pressure projection method for non-isothermal flows is introduced and ISPH discretisation is presented and PPE is discussed. In Section 5, results are provided. Effect of $Ra$ number on flow field is investigated and validation of the method is presented. Finally, conclusions are drawn in Section 6.

## 2. Mathematical modelling

Natural convection in a square cavity is modelled by assigning constant temperatures on vertical walls and adiabatic boundary conditions on horizontal walls. Throughout the simulations, gravity is in negative *y direction* and Boussinesq approximation is used. Problem geometry is provided in Figure 1.

For incompressible Newtonian natural convection problems, governing equations are continuity, momentum and energy equations. Then, in Eulerian form, governing equations for a non-isothermal Newtonian flow with Boussinesq approximation is written as

$$\nabla \cdot \mathbf{u} = 0 \tag{1}$$

$$\frac{\partial \mathbf{u}}{\partial t} + \mathbf{u} \cdot \nabla \mathbf{u} = -\frac{1}{\rho}\nabla p + \nu \nabla^2 \mathbf{u} + \mathbf{g}\left(\beta_T \left(T - T_0\right)\right) \tag{2}$$

$$\frac{\partial T}{\partial t} + \mathbf{u} \cdot \nabla T = \alpha \nabla^2 T. \tag{3}$$

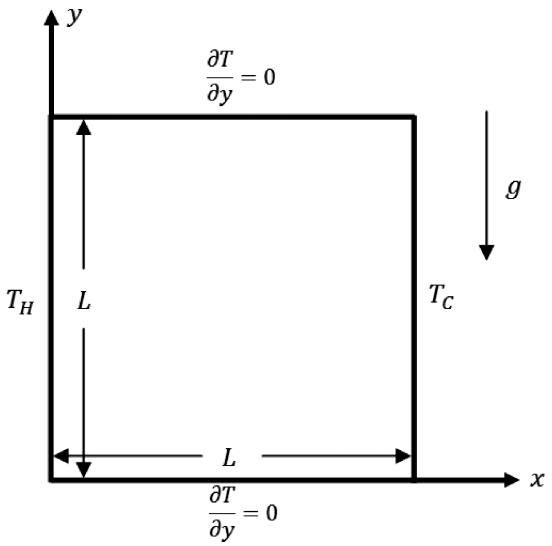


Figure 1. Geometry of natural convection in a square cavity.

Equations (2) and (3) are non-dimensionalised using the following dimensionless variables:

$$(x^*, y^*) = \frac{(x, y)}{L} \tag{4}$$

$$\mathbf{u}^* = \mathbf{u}\frac{L}{\alpha} \tag{5}$$

$$T^* = \frac{T - T_C}{T_H - T_C} \tag{6}$$

$$p^* = p\frac{L^2}{\rho\alpha^2} \tag{7}$$

$$Pr = \frac{\nu}{\alpha} \tag{8}$$

$$Ra = \frac{g\beta_T\,(T_H - T_C)\,L^3}{\nu\,\alpha}, \tag{9}$$

where $L$ is a characteristic length, $T_H$ is the maximum temperature, $T_C$ is the minimum temperature, $Pr$ is Prandtl number and $Ra$ is Rayleigh number. Then, Equations (2) and (3) reduce to

$$\frac{\partial \mathbf{u}^*}{\partial t} + \mathbf{u}^* \cdot \nabla \mathbf{u}^* = -\nabla p^* + Pr\,\nabla^2 \mathbf{u}^* + Ra\,Pr\,(T^* - 0.5)\,\hat{\mathbf{g}} \tag{10}$$

$$\frac{\partial T^*}{\partial t} + \mathbf{u}^* \cdot \nabla\, T^* = \nabla^2\, T^*. \tag{11}$$

In Equation (10), $\hat{\mathbf{g}}$ represents unit vector for gravity.

## 3. SPH methodology

SPH is derived from integral representation of any scalar function, $f(\mathbf{r})$, defined on a three-dimensional coordinate system using Dirac delta function,

$$f(\mathbf{r}) = \int_\forall f(\mathbf{r}')\delta(\mathbf{r} - \mathbf{r}')\,d\mathbf{r}', \tag{12}$$

where $\delta(\mathbf{r} - \mathbf{r}')$ is the Dirac delta function and $\forall$ is the volume over which $d\mathbf{r}'$ is ranging. Dirac delta function, $\delta(\mathbf{r} - \mathbf{r}')$, is approximated by a smoothing kernel $W(\mathbf{r} - \mathbf{r}', h)$,

$$\delta(\mathbf{r} - \mathbf{r}') = \lim_{h\to 0} W(\mathbf{r} - \mathbf{r}', h), \tag{13}$$

where $h$ is the smoothing length that confines neighbourhood of particles. Smoothing kernel, $W(\mathbf{r} - \mathbf{r}', h)$, is subjected to normalisation condition:

$$\int_\forall W(\mathbf{r} - \mathbf{r}', h)\,d\mathbf{r}' = 1. \tag{14}$$

For symmetric smoothing kernels, $W(\mathbf{r} - \mathbf{r}', h) = W(\mathbf{r}' - \mathbf{r}, h)$, by expanding $W(\mathbf{r} - \mathbf{r}', h)$ in Taylor series, Equation (12) can be approximated as

$$f(\mathbf{r}) = \int_\forall f(\mathbf{r}')W(\mathbf{r} - \mathbf{r}', h)\,d\mathbf{r}' + \mathcal{O}(h^2). \tag{15}$$

Multiplying and dividing the integrand in Equation (15) by $\rho(\mathbf{r}')$, an equivalent expression to Equation (15) is obtained

$$f(\mathbf{r}) = \int_\forall \frac{f(\mathbf{r}')}{\rho(\mathbf{r}')}W(\mathbf{r} - \mathbf{r}', h)\,\rho(\mathbf{r}')d\mathbf{r}' + \mathcal{O}(h^2). \tag{16}$$

Since SPH discretises a continuum onto a set of particles of mass, $m' = \rho(r')dr'$, Equation (16) becomes the famous SPH summation formula,

$$f_i = \sum_j \frac{m_j}{\rho_j} f_j W_{ij}, \tag{17}$$

where $f_i = f(\mathbf{r}_i)$, $W_{ij} = W(\mathbf{r}_i - \mathbf{r}_j, h)$ and any difference of a certain parameter, $f$, corresponding to two different particles is shown using the notation $f_{ij} = f_i - f_j$. A function can be calculated at a particle $i$ using Equation (17). For instance, density of a particle $i$ is calculated as

$$\rho_i = \sum_j m_j W_{ij}. \tag{18}$$

In this paper, we use quintic kernel due to Schoenberg (1946)

$$W_{ij} = \frac{3}{478\pi}\begin{cases} (3-q)^5 - 6(2-q)^5 + 15(1-q)^5, & 0 \le q \le 1 \\ (3-q)^5 - 6(2-q)^5, & 1 \le q \le 2 \\ (3-q)^5, & 2 \le q \le 3 \\ 0, & 3 \le q, \end{cases} \tag{19}$$

where $q = \frac{r_{ij}}{h}$. A comprehensive discussion on effect of kernel types and properties, especially on particle disorder, can be found in Dehnen and Aly (2012).

Moreover, SPH can be used to discretise mathematical operators such as derivative, divergence, gradient and Laplacian operators. In the following sections, SPH discretisation of these operators is discussed.

### 3.1. SPH form of mathematical operators

Governing equations describing a physical phenomenon usually include mathematical operators such as derivative, gradient, divergence and Laplacian operators. Like other computational methods, SPH can approximate these operators.

#### 3.1.1. SPH derivative operator

SPH derivative operator is obtained from differentiating Equation (15),

$$\frac{\partial}{\partial r} f(\mathbf{r}) = \frac{\partial}{\partial r} \int_{\forall} f(\mathbf{r}') W(\mathbf{r} - \mathbf{r}', h)\, d\mathbf{r}' \tag{20}$$

$$= \int_{\forall} f(\mathbf{r}') \frac{\partial W(\mathbf{r} - \mathbf{r}', h)}{\partial r}\, d\mathbf{r}'. \tag{21}$$

Discretising Equation (20) similar to Equation (15), SPH derivative operator is obtained as

$$\frac{\partial f_i}{\partial r_i} = \sum_j \frac{m_j}{\rho_j} f_j \frac{\partial W_{ij}}{\partial r_i}. \tag{22}$$

Furthermore, smoothing kernel must be a normalised function,

$$1 = \sum_j \frac{m_j}{\rho_j} W_{ij}. \tag{23}$$

Then, derivative of '1' is calculated as

$$0 \approx \frac{\partial(1)}{\partial r_i} = \sum_j \frac{m_j}{\rho_j} \frac{\partial W_{ij}}{\partial r_i}. \tag{24}$$

Therefore, there is an error associated with the derivative of a constant function. Thus, considering

$$\frac{\partial(f \cdot 1)}{\partial r} = \frac{\partial(f)}{\partial r} \cdot 1 + \frac{\partial 1}{\partial r} \cdot f \tag{25}$$

$$\frac{\partial f}{\partial r} = \frac{\partial f}{\partial r} - \frac{\partial 1}{\partial r} \tag{26}$$

accuracy of SPH derivative operator is increased by taking the errors associated with the derivative of '1' into account

$$\frac{\partial f_i}{\partial r_i} = \sum_j \frac{m_j}{\rho_j} (f_j - f_i) \frac{\partial W_{ij}}{\partial r_i}. \tag{27}$$

This procedure can be generalised by differentiation $\frac{\partial}{\partial r}(f\rho^n) = \rho^n \frac{\partial f}{\partial r} + nf\rho^{n-1} \frac{\partial \rho}{\partial r}$. Thus,

$$\frac{\partial f_i}{\partial r_i} = \frac{1}{\rho_i^n} \left( \frac{\partial}{\partial r_i} (f_i \rho_i^{n-1}) - n f_i \rho_i^{n-1} \frac{\partial \rho_i}{\partial r_i} \right) \tag{28}$$

$$= \frac{1}{\rho_i^n} \sum_j m_j \left( f_j \rho_j^{n-1} - n f_i \rho_i^{n-1} \right) \frac{\partial W_{ij}}{\partial r_i}. \tag{29}$$

Two commonly used SPH derivative operators are obtained for $n = 1$ and $n = -1$. For $n = 1$, SPH derivative operator becomes

$$\frac{\partial f_i}{\partial r_i} = \frac{1}{\rho_i} \sum_j m_j \left( f_j - f_i \right) \frac{\partial W_{ij}}{\partial r_i}. \tag{30}$$

For $n = -1$, SPH derivative operator becomes

$$\frac{\partial f_i}{\partial r_i} = \rho_i \sum_j m_j \left( \frac{f_i}{\rho_i^2} + \frac{f_j}{\rho_j^2} \right) \frac{\partial W_{ij}}{\partial r_i}. \tag{31}$$

For constant function, Equation (30) results identically in '0' while Equation (31) does not. In this study, Equation (30) is used.

#### 3.1.2. SPH gradient operator

Similar to the SPH derivative operator, there are two types of SPH gradient operator commonly used in SPH literature,

$$(\nabla f)_i = \frac{1}{\rho_i} \sum_j m_j \left( f_j - f_i \right) \nabla_i W_{ij} \tag{32}$$

$$(\nabla f_i) = \rho_i \sum_j m_j \left( \frac{f_i}{\rho_i^2} + \frac{f_j}{\rho_j^2} \right) \nabla_i W_{ij}. \tag{33}$$

In the SPH literature, Equation (33) is commonly used in discretisation of pressure gradient term since this operator is symmetric and conserves linear momentum. However, Equation (32) is used in this study. Although Equation (32) does not conserve linear momentum, it results in more accurate approximations than Equation (33).

#### 3.1.3. SPH divergence operator

Like SPH gradient operator, SPH divergence operator can be constructed as follows:

$$(\nabla \cdot \mathbf{f})_i = \frac{1}{\rho_i} \sum_j m_j \left( \mathbf{f}_j - \mathbf{f}_i \right) \cdot \nabla_i W_{ij} \tag{34}$$

$$(\nabla \cdot \mathbf{f})_i = \rho_i \sum_j m_j \left( \frac{\mathbf{f}_i}{\rho_i^2} + \frac{\mathbf{f}_j}{\rho_j^2} \right) \cdot \nabla_i W_{ij}. \tag{35}$$

In this study, Equation (34) is used.

*3.1.4. SPH Laplacian operator*

Laplacian operator usage differs from gradient and divergence operators in the SPH literature. The simplest SPH Laplacian operator is

$$(\nabla^2 f)_i = \sum_j \frac{m_j}{\rho_j} f_j \nabla^2 W_{ij}. \tag{36}$$

Another form of SPH Laplacian operator is called Approximate Laplacian operator,

$$(\nabla^2 f)_i = \sum_j 2\frac{m_j}{\rho_j} \frac{\mathbf{r}_{ij} \cdot \nabla W_{ij}}{|\mathbf{r}_{ij}|^2 + \eta^2} f_{ij}, \tag{37}$$

where $\eta$ is a very small number in order to prevent a zero denominator. Approximate Laplacian operator was first used in Cleary and Monaghan (1999) and it is one of the most commonly used SPH Laplacian operators. It combines finite difference and SPH derivative operators.

### *3.2. High-order approximation schemes in SPH*

In Lagrangian SPH approach, one of the most significant problems is that uniformity of particle distribution is not conserved exactly during simulations. As a consequence, inaccuracies arise as a kernel and its derivatives are discretised. To remedy these, correction techniques for the kernel and its derivatives were developed (Randles and Libersky 1996; Dilts 1999; Chen and Beraun 2000; Oger et al. 2007). An instructive summary of these techniques is presented in Liu and Liu (2010) and Gomez-Gesteira et al. (2012).

In the proceeding subsection, correction methods used in SPH method are given systematically and behaviour of those corrections on uniformly distributed grids will be discussed in detail.

*3.2.1. Density field correction*

*3.2.1.1. Shepard filter.* This is a 'zeroth-order' correction technique. It is very simple to implement. It is based on normalisation on smoothing kernel $W$. In SPH, density of a particle is calculated by

$$\rho_i = \sum_j m_j W_{ij}. \tag{38}$$

However, smoothing kernel usually does not satisfy the normalisation condition,

$$1 = \sum_j \frac{m_j}{\rho_j} W_{ij}. \tag{39}$$

As a consequence, density field calculated by Equation (38) is inaccurate. To increase accuracy of density field, a corrected smoothing kernel is calculated by

$$\tilde{W}_{ij} = \frac{W_{ij}}{\sum_j \frac{m_j}{\rho_j} W_{ij}}. \tag{40}$$

Then, corrected density field is calculated by inserting corrected smoothing kernel $\tilde{W}_{ij}$ into Equation (39),

$$\rho_i^{\text{corrected}} = \sum_j m_j \tilde{W}_{ij.} \tag{41}$$

**Note:** In grid-based SPH, Equation (39) holds. Therefore, denominator in Equation (40) is equal to 1. Therefore, the following relation holds:

$$\tilde{W}_{ij} = W_{ij}. \tag{42}$$

As a consequence, $\rho_i^{\text{corrected}}$ and $\rho_i$ are identical,

$$\rho_i^{\text{corrected}} = \rho_i \tag{43}$$

Thus, in grid-based SPH, usage of the Shepard filter is unnecessary.

*3.2.1.2. Moving Least Squares (MLS).* This is a first-order correction approach. It is similar to Shepard filter in terms of calculating a new smoothing kernel $W_{ij}^{\text{MLS}}$,

$$\rho_i = \sum_j m_j W_{ij}^{\text{MLS}}, \tag{44}$$

where $W_{ij}^{\text{MLS}}$ is calculated by

$$W_{ij}^{\text{MLS}} = \vec{\beta} \cdot (\vec{r}_i - \vec{r}_j) W_{ij}. \tag{45}$$

In Equation (45), $\vec{\beta}$ is a vector estimated by

$$\vec{\beta} = \begin{bmatrix} \beta_1 \\ \beta_2 \\ \beta_3 \end{bmatrix} = \mathbf{A}^{-1} \begin{bmatrix} 1 \\ 0 \\ 0 \end{bmatrix} \tag{46}$$

and $\mathbf{A}$ is a matrix obtained by

$$\mathbf{A} = \sum_j \frac{m_j}{\rho_j} \tilde{\mathbf{A}} W_{ij}, \tag{47}$$

where $\tilde{\mathbf{A}}$ is

$$\tilde{\mathbf{A}} = \begin{bmatrix} 1 & (x_i - x_j) & (y_i - y_j)(x_i - x_j) \\ (x_i - x_j)^2(x_i - x_j) & (y_i - y_j)(y_i - y_j) & (x_i - x_j)(y_i - y_j) \\ (y_i - y_j)^2 & & \end{bmatrix}. \tag{48}$$

For a 2-D problem, $W_{ij}^{\mathrm{MLS}}$ is calculated by

$$W_{ij}^{\mathrm{MLS}} = \left(\beta_1 + \beta_2(x_i - x_j) + \beta_3(y_i - y_j)\right) W_{ij}. \tag{49}$$

**Note:** In grid-based SPH, $\mathbf{A}$ is calculated by using a normalised symmetric kernel $W_{ij}$. Therefore,

$$\begin{aligned}
\mathbf{A}_{11} &= \sum_j \frac{m_j}{\rho_j} W_{ij} = 1 \\
\mathbf{A}_{12} &= \sum_j \frac{m_j}{\rho_j}(x_i - x_j) W_{ij} = 0 \\
\mathbf{A}_{13} &= \sum_j \frac{m_j}{\rho_j}(y_i - y_j) W_{ij} = 0 \\
\mathbf{A}_{21} &= \sum_j \frac{m_j}{\rho_j}(x_i - x_j) W_{ij} = 0 \\
\mathbf{A}_{22} &= \sum_j \frac{m_j}{\rho_j}(x_i - x_j)^2 W_{ij} \neq 0 \\
\mathbf{A}_{23} &= \sum_j \frac{m_j}{\rho_j}(x_i - x_j)(y_i - y_j) W_{ij} = 0 \\
\mathbf{A}_{31} &= \sum_j \frac{m_j}{\rho_j}(y_i - y_j) W_{ij} = 0 \\
\mathbf{A}_{32} &= \sum_j \frac{m_j}{\rho_j}(x_i - x_j)(y_i - y_j) W_{ij} = 0 \\
\mathbf{A}_{33} &= \sum_j \frac{m_j}{\rho_j}(y_i - y_j)^2 W_{ij} \neq 0.
\end{aligned} \tag{50}$$

Therefore, we obtain $\mathbf{A}$ as

$$\mathbf{A} = \begin{bmatrix} 1 & 0 & 0 \\ 0 & c_1 & 0 \\ 0 & 0 & c_2 \end{bmatrix}, \tag{51}$$

where $c_1$ and $c_2$ are some values estimated for $\mathbf{A}_{22}$ and $\mathbf{A}_{33}$. To calculate $\vec{\beta}$, we need to calculate the inverse of $\mathbf{A}$, which is a very simple task,

$$\mathbf{A}^{-1} = \begin{bmatrix} 1 & 0 & 0 \\ 0 & d_1 & 0 \\ 0 & 0 & d_2 \end{bmatrix}, \tag{52}$$

where $d_1$ and $d_2$ are values satisfying $c_1 \cdot d_1 = 1$ and $c_2 \cdot d_2 = 1$, respectively. Having obtained $\mathbf{A}^{-1}$, we can calculate $\vec{\beta}$

$$\vec{\beta} = \begin{bmatrix} 1 & 0 & 0 \\ 0 & d_1 & 0 \\ 0 & 0 & d_2 \end{bmatrix} \begin{bmatrix} 1 \\ 0 \\ 0 \end{bmatrix} = \begin{bmatrix} 1 \\ 0 \\ 0 \end{bmatrix}. \tag{53}$$

Thus,

$$\begin{aligned}
W_{ij}^{\mathrm{MLS}} &= (\beta_1 + \beta_2(x_i - x_j) + \beta_3(y_i - y_j)) W_{ij} \\
&= \beta_1 W_{ij} \\
&= W_{ij}.
\end{aligned} \tag{54}$$

Thus, in grid-based SPH, MLS correction is unnecessary.

### 3.2.2. Kernel correction

This is very similar to Shepard filter. In SPH, a function $f_i$ is calculated by

$$f_i = \sum_j \frac{m_j}{\rho_j} f_j W_{ij}. \tag{55}$$

However, when particle consistency degrades, Equation (55) inaccurately approximates $f_i$. Therefore, Equation (55) is normalised by

$$f_i = \frac{\sum_j \frac{m_j}{\rho_j} f_j W_{ij}}{\sum_j \frac{m_j}{\rho_j} W_{ij}}. \tag{56}$$

**NOTE:** In grid-based SPH, since a normalised symmetric kernel $W_{ij}$ is used, we have

$$\begin{aligned}
f_i &= \frac{\sum_j \frac{m_j}{\rho_j} f_j W_{ij}}{\sum_j \frac{m_j}{\rho_j} W_{ij}} \\
&= \sum_j \frac{m_j}{\rho_j} f_j W_{ij}.
\end{aligned} \tag{57}$$

Therefore, kernel correction is unnecessary in the grid-based SPH.

### 3.2.3. Kernel gradient correction

Since governing equations of fluid mechanics involve terms including taking gradients, approximation of gradients is a significant task in terms of accuracy. In SPH, kernel gradients are used in calculation of gradients of terms in governing equations. However, when particle consistency degrades, conventional approaches in kernel gradient calculation produce errors. To prevent this, kernel gradient should be normalised. The normalised kernel gradient is calculated by

$$\nabla \tilde{W}_{ij} = \mathbf{L}^{-1} \nabla W_{ij}, \tag{58}$$

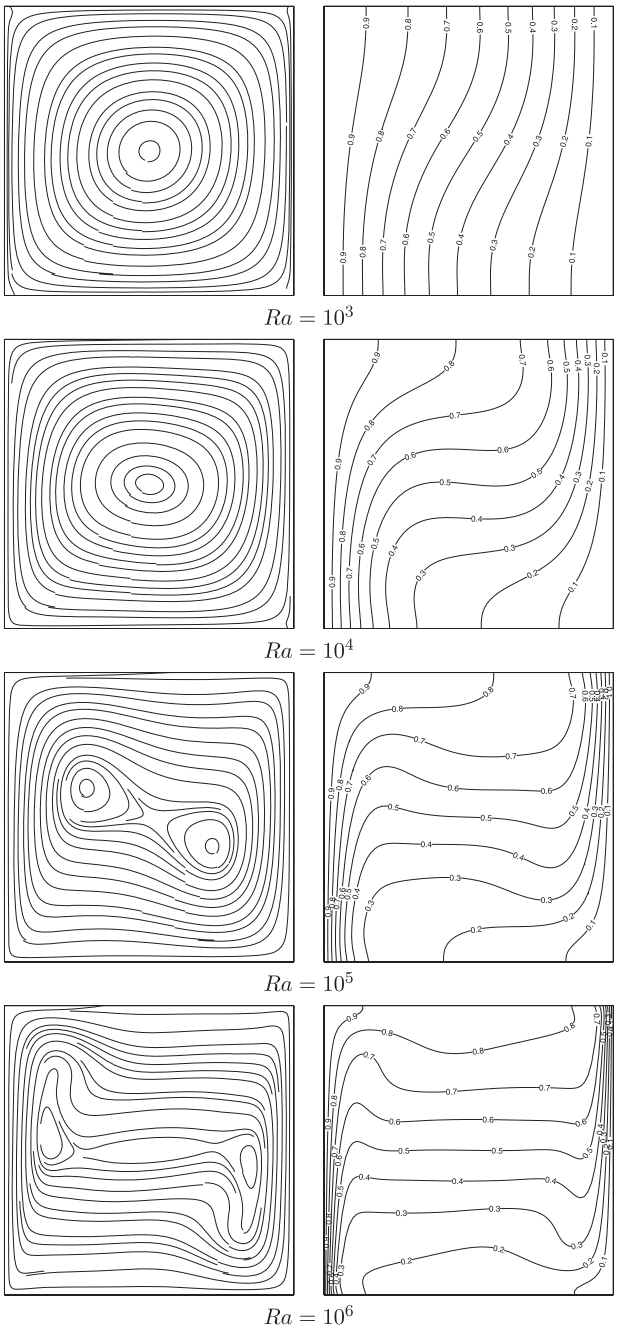


Figure 2. (a) Streamlines and (b) temperature profiles at $Ra = 10^3 - 10^6$.

where $\mathbf{L}$ is a matrix

$$\mathbf{L} = \begin{bmatrix} \sum_j \frac{m_j}{\rho_j}(x_j - x_i)\frac{\partial W_{ij}}{\partial x_i} & \sum_j \frac{m_j}{\rho_j}(x_j - x_i)\frac{\partial W_{ij}}{\partial y_i} \\ \sum_j \frac{m_j}{\rho_j}(y_j - y_i)\frac{\partial W_{ij}}{\partial x_i} & \sum_j \frac{m_j}{\rho_j}(y_j - y_i)\frac{\partial W_{ij}}{\partial y_i} \end{bmatrix}. \quad (59)$$

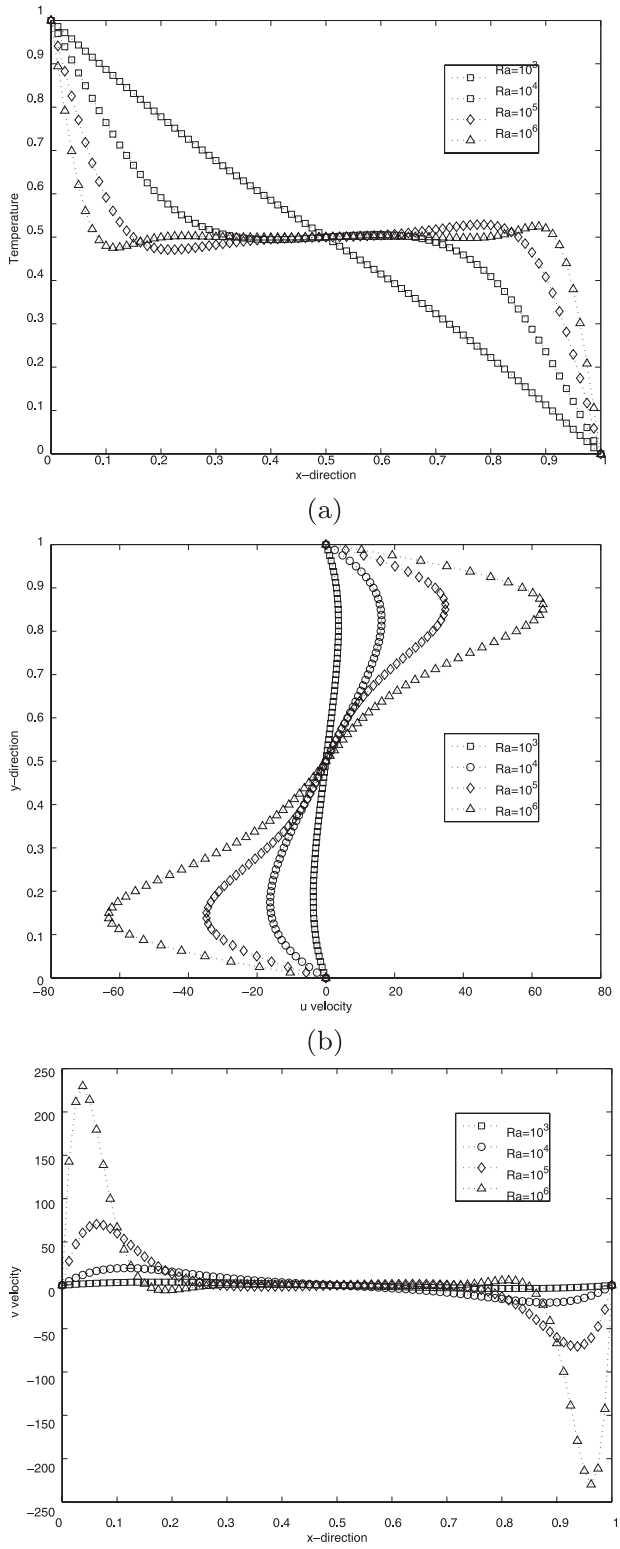


Figure 3. (a) Temperature profiles in $x$ direction at half width, (b) velocity profiles in $x$-direction at half width, (c) velocity profiles in $y$-direction at half height from $Ra = 10^3$ to $Ra = 10^6$.

**NOTE:** In the grid-based SPH, we have

$$\begin{aligned} L_{11} &= \sum_j \frac{m_j}{\rho_j}(x_j - x_i)\frac{\partial W_{ij}}{\partial x_i} = 1 \\ L_{12} &= \sum_j \frac{m_j}{\rho_j}(x_j - x_i)\frac{\partial W_{ij}}{\partial y_i} = 0 \\ L_{21} &= \sum_j \frac{m_j}{\rho_j}(y_j - y_i)\frac{\partial W_{ij}}{\partial x_i} = 0 \\ L_{22} &= \sum_j \frac{m_j}{\rho_j}(y_j - y_i)\frac{\partial W_{ij}}{\partial y_i} = 1. \end{aligned} \tag{60}$$

In matrix representation, we have

$$\mathbf{L} = \begin{bmatrix} 1 & 0 \\ 0 & 1 \end{bmatrix}, \tag{61}$$

which is the identity matrix. Inserting this into Equation (58), we obtain

$$\nabla \tilde{W}_{ij} = \nabla W_{ij}. \tag{62}$$

As a conclusion, kernel gradient correction technique is unnecessary in the grid-based SPH technique as in previous correction techniques. It is worth noting that ineffectiveness of these correction techniques in grid-based SPH is independent of kernel types and properties. Therefore, kernel types and properties do not have any effect on the results except for discretisation error. However, in conventional SPH techniques, kernel type and properties have influenced particle disorder and thus, they have a significant effect on the results (Dehnen and Aly 2012).

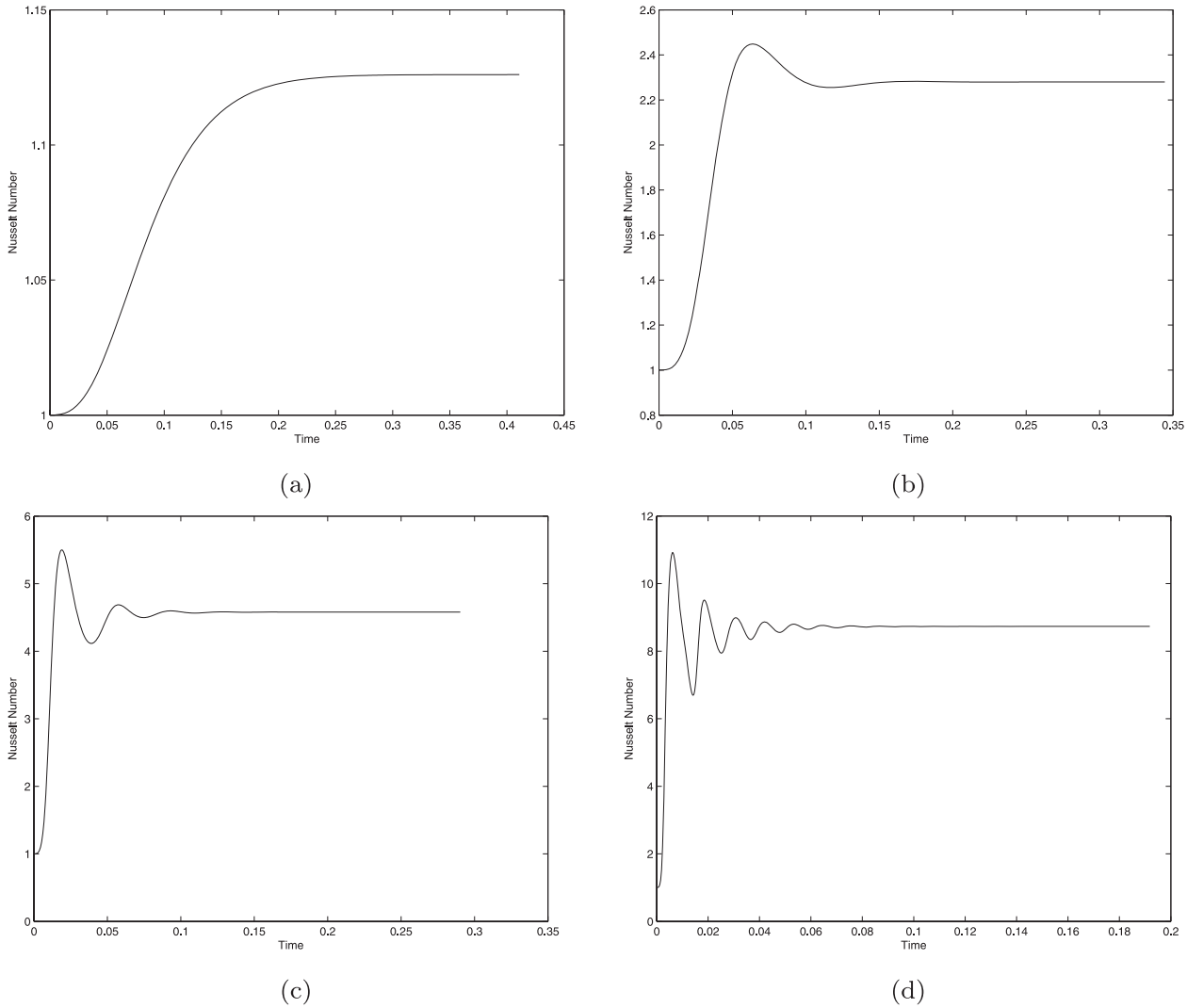


Figure 4. $Nu_m$ values on the hot wall for (a) $Ra = 10^3$, (b) $Ra = 10^2$, (c) $Ra = 10^5$ and (d) $Ra = 10^6$.

## 4. ISPH formulation of governing equations

SPH discretises governing equations of fluid mechanics by the operators discussed in Section 3. Like all numerical methods that deal with primitive flow variables, pressure is one of the most challenging variables for SPH to solve. In ISPH method, pressure projection method is used to solve the flow field in this study. Using the projection method, momentum equation (10) is rewritten as

$$\frac{\mathbf{u}^{n+1}-\mathbf{u}^{n}}{\Delta t}+\mathbf{u}^{n}\cdot\nabla\mathbf{u}^{n}=-\nabla p+Pr\,\nabla^{2}\mathbf{u}^{n}+RaPr(T^{n}-0.5). \quad (63)$$

An intermediate velocity term $\mathbf{u}^{*}$ is added and subtracted from the nominator of the left-hand side of Equation (63),

$$\frac{\mathbf{u}^{n+1}-\mathbf{u}^{n}}{\Delta t}=\frac{(\mathbf{u}^{n+1}-\mathbf{u}^{*})+(\mathbf{u}^{*}-\mathbf{u}^{n})}{\Delta t}. \quad (64)$$

The intermediate velocity $\mathbf{u}^{*}$ is calculated without the gradient of pressure term in Equation (63),

$$\mathbf{u}^{*}=\mathbf{u}^{n}+\Delta t\,(Pr\nabla^{2}\mathbf{u}^{n}-\mathbf{u}^{n}\cdot\nabla\mathbf{u}^{n}+RaPr(T^{n}-0.5)). \quad (65)$$

Therefore, velocity at time step $n+1$ is calculated as

$$\mathbf{u}^{n+1}=\mathbf{u}^{*}-\Delta t\nabla p^{n+1}. \quad (66)$$

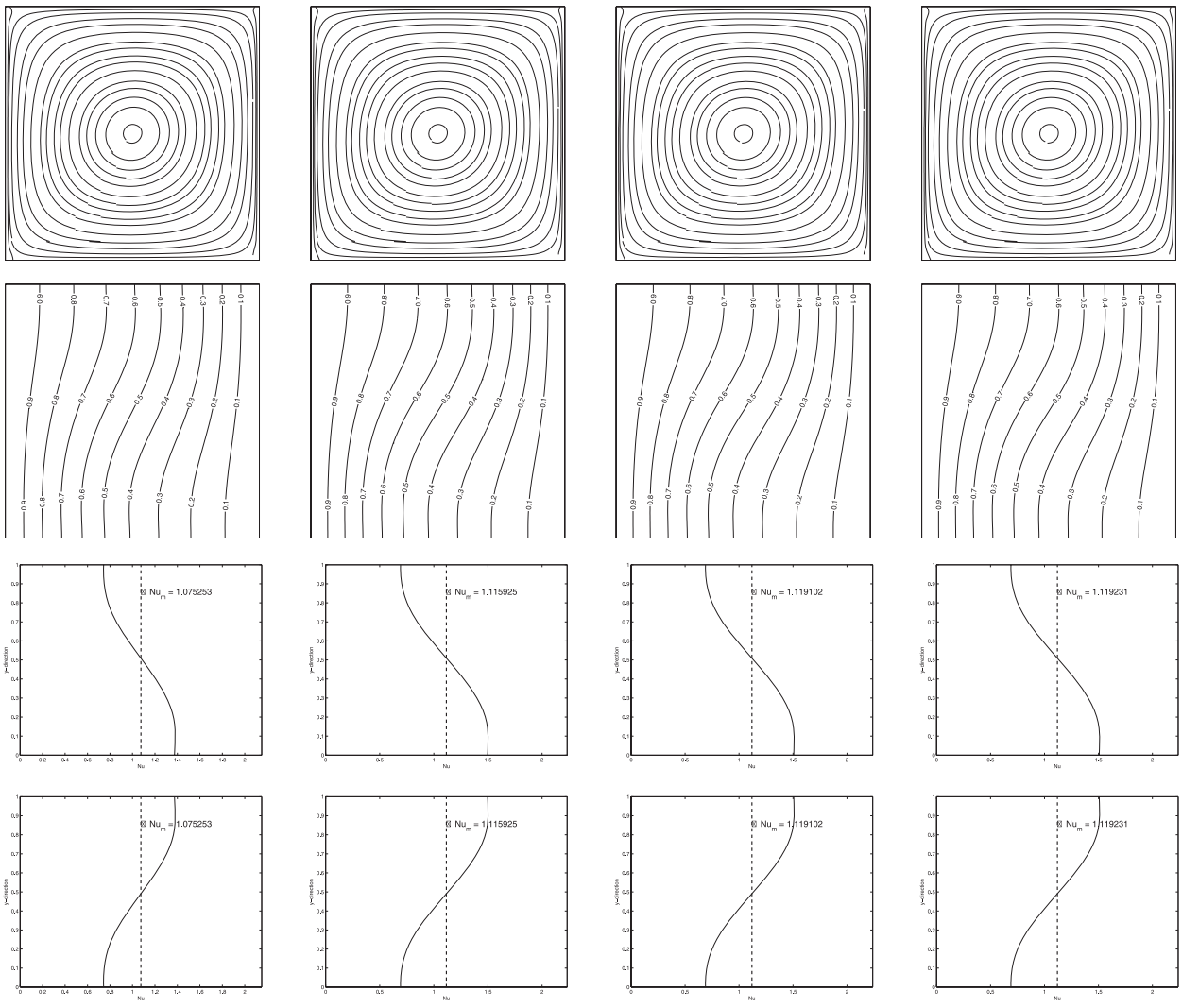


(a) $t = 0.1$ (b) $t = 0.2$ (c) $t = 0.3$ (d) $t = 0.4$

Figure 5. Evolution of streamlines, temperature profiles and $Nu$ number profiles at the hot and cold walls (from top to down) in time at $Ra = 10^{3}$.

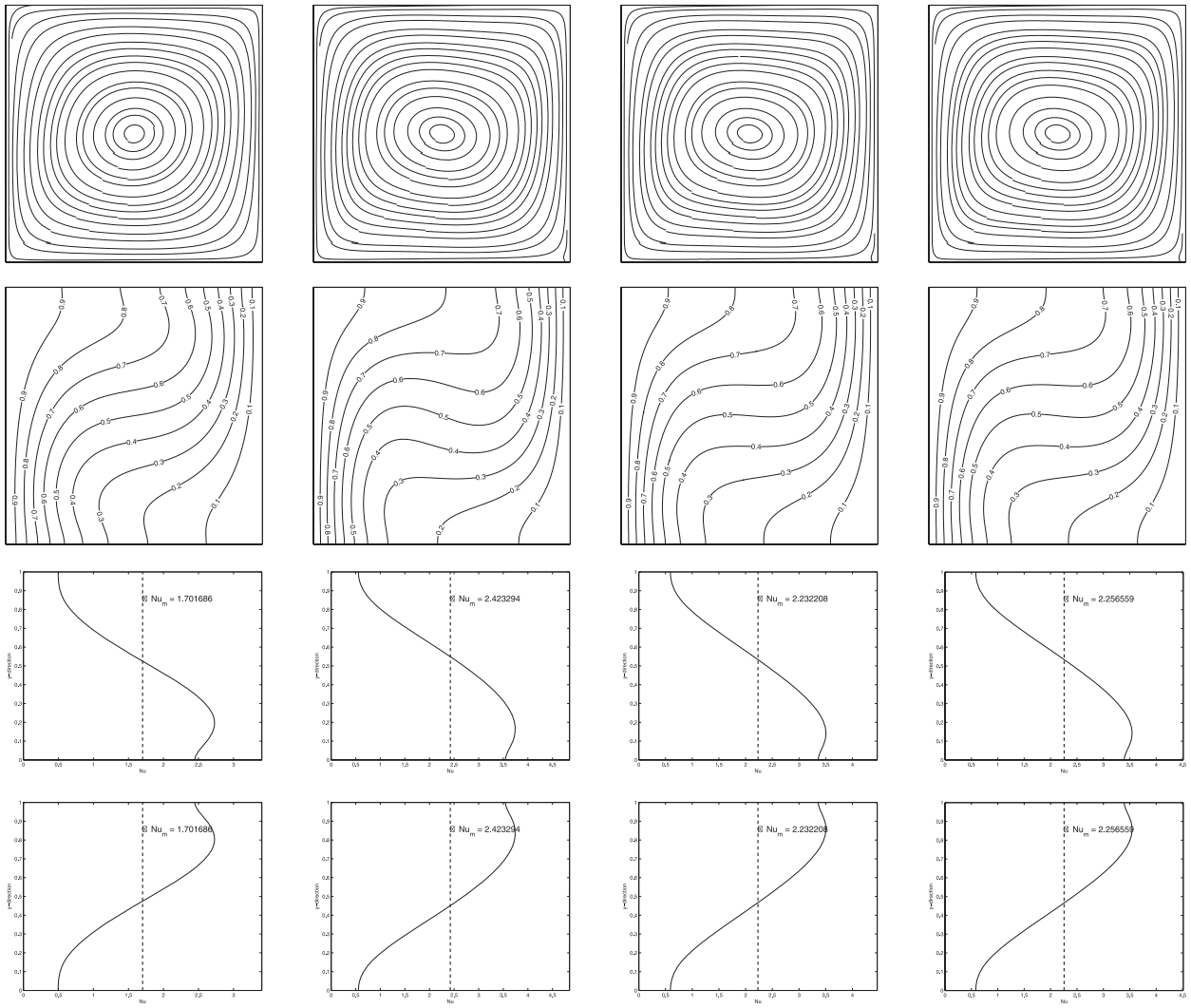


(a) $t = 0.0342$ (b) $t = 0.0638$ (c) $t = 0.1170$ (d) $t = 0.3446$

Figure 6. Evolution of streamlines, temperature profiles and $Nu$ number profiles at the hot and cold walls (from top to down) in time at $Ra = 10^4$.

Since $\mathbf{u}^{n+1}$ is a divergence-free velocity, taking divergence of Equation (66), PPE is obtained,

$$\nabla^2 p^{n+1} = \frac{\nabla \cdot \mathbf{u}^*}{\Delta t}. \tag{67}$$

After obtaining pressure, velocity at the next time step $\mathbf{u}^{n+1}$ is found by Equation (66). Temperature $T^{n+1}$ is calculated explicitly by Heun's method as

$$T^{n+1} = T^n + \frac{\Delta t}{2}((\nabla^2 T^n - \mathbf{u}^n \cdot \nabla T^n) + (\nabla^2 \widetilde{T}^{n+1} - \mathbf{u}^{n+1} \cdot \nabla \widetilde{T}^{n+1})), \tag{68}$$

where $\widetilde{T}^{n+1}$ is estimated by

$$\widetilde{T}^{n+1} = T^n + \Delta t(\nabla^2 T^n - \mathbf{u}^n \cdot \nabla T^n). \tag{69}$$

The procedure presented here is repeated until a steady state is reached.

## 5. Results and discussion

Laminar transient natural convection in a square cavity is studied using ISPH on $81 \times 81$ uniform Eulerian grids. Initially, velocities are zero and the temperature is linearly decreased in $x$ direction. Effect of $Ra$ on Nusselt number, temperature and velocity fields is investigated from $Ra = 10^3$ to $Ra = 10^6$. Original results obtained from the

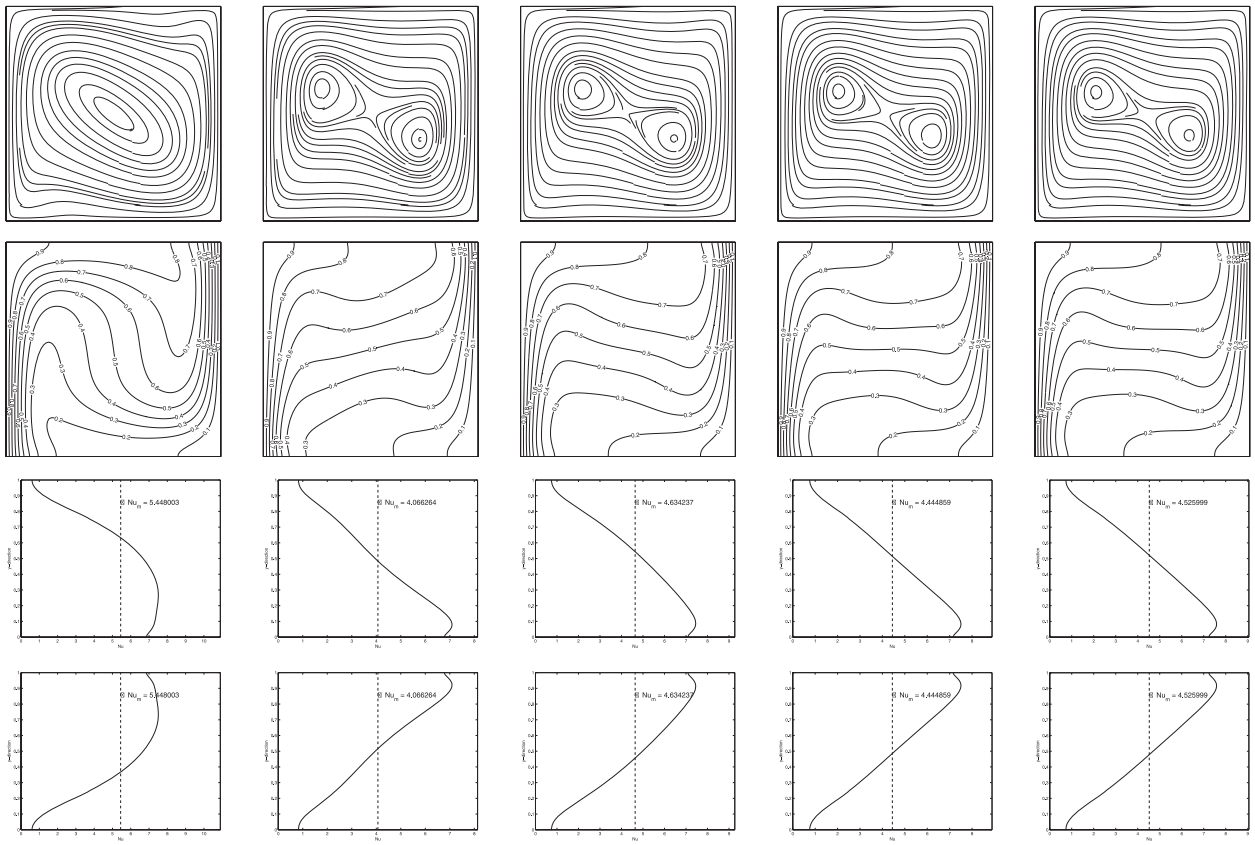


(a) $t = 0.0190$ (b) $t = 0.0391$ (c) $t = 0.0575$ (d) $t = 0.0745$ (e) $t = 0.2904$

Figure 7. Evolution of streamlines, temperature profiles and $Nu$ number profiles at the hot and cold walls (from top to down) in time at $Ra = 10^5$.

simulations are tabulated and compared to available data in the literature.

### *5.1. Effect of Rayleigh number*

The effect on Rayleigh number is investigated on $81 \times 81$ grids. In Figure 2, streamlines and temperature contours are presented for $Ra$ numbers between $10^3$ and $10^6$. For low $Ra$ numbers, streamlines include only one primary vortex. As $Ra$ number increases, especially for $Ra = 10^5$, secondary vortices occur towards the upper-left and lower-right corners. For high $Ra$ numbers, especially for $Ra = 10^6$, secondary vortices near the upper-left and lower-right corners approach the left and right walls, respectively, and an additional secondary vortex appears in the middle of the cavity. Velocity values near the walls are higher compared to velocity values in the near neighbourhood of the centre of the cavity.

Moreover, temperature contours are almost vertical for low $Ra$ number simulations. For $Ra = 10^3$, the temperature decreases almost linearly in a positive $x$ direction. As $Ra$ number increases, temperature contours become more and more horizontal. For instance, temperature contours are almost horizontal in the central region of the cavity for $Ra = 10^6$. This can also be seen in Figure 3.

Furthermore, in Figure 3, it can be observed that maximum velocities exist near the walls and minimum velocities exist in the middle region of the cavity. Since left and right walls are the locations of global maxima and minima for temperature, location of peaks in $v$-velocity profile must be closer to walls than the location of peaks in $u$-velocity profile, which is also observed in Figure 3.

In addition to analysis of temperature and velocity distribution in the system at the steady state, we would like to identify time evolution of $Nu_m$ on the side walls (hot and cold sides) as shown in Figure 4. As $Ra$ number is increased, response of $Nu_m$ becomes more oscillatory and transient time to reach steady state is decreased. At $Ra = 10^3$, $Nu_m$ reaches steady state asymptotically and time rate of change of $Nu_m$ is always greater than or equal to 0. However, at $Ra = 10^4$, $Nu_m$ makes a peak and then decreases to its steady-state value asymptotically. At $Ra = 10^5$, $Nu_m$ becomes oscillatory but it is damped out and then it reaches a steady state. Finally, at $Ra = 10^6$, $Nu_m$ exhibits more

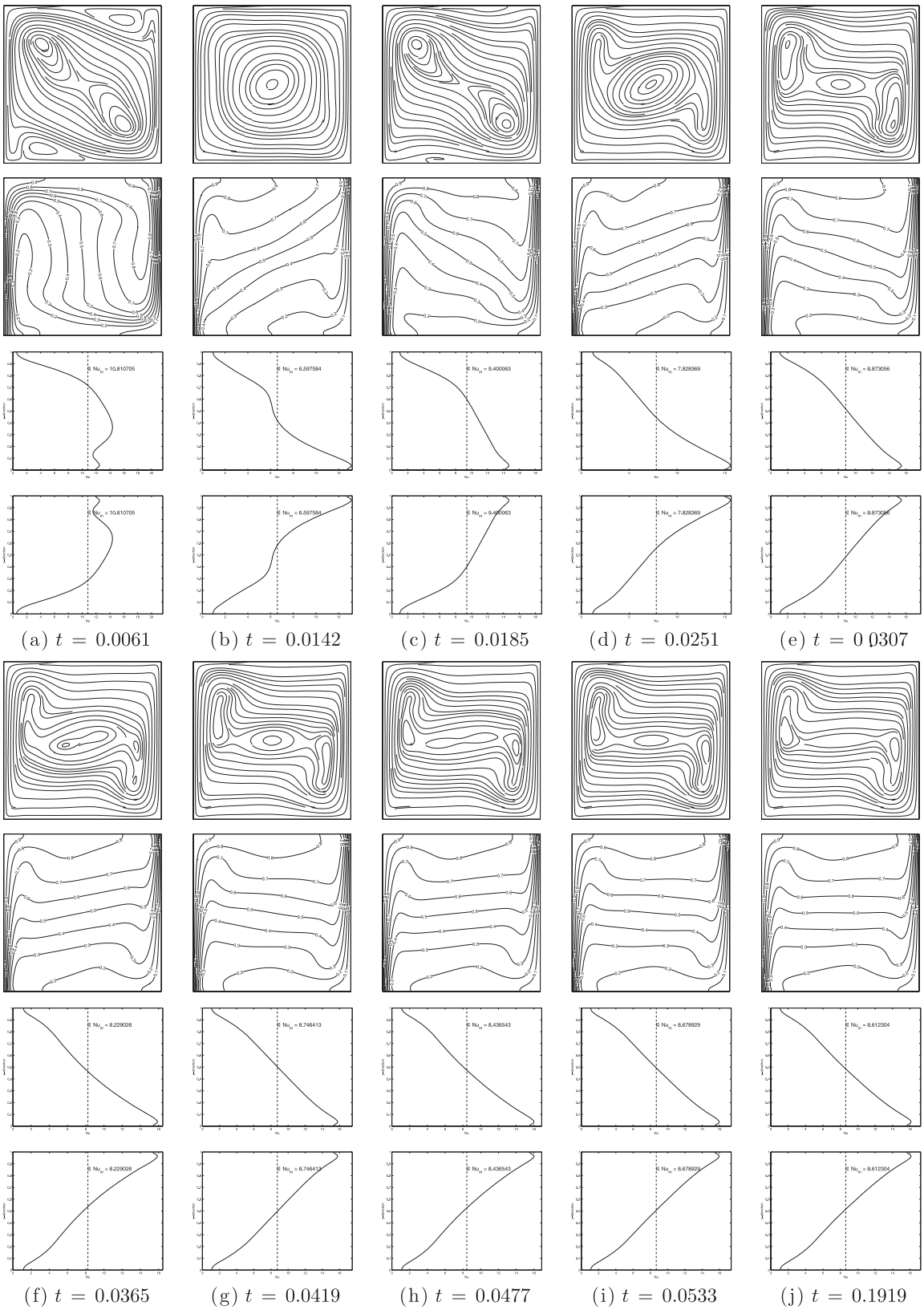

(a) $t = 0.0061$ (b) $t = 0.0142$ (c) $t = 0.0185$ (d) $t = 0.0251$ (e) $t = 0\ 0307$

(f) $t = 0.0365$ (g) $t = 0.0419$ (h) $t = 0.0477$ (i) $t = 0.0533$ (j) $t = 0.1919$

Figure 8. Evolution of streamlines, temperature profiles and $Nu$ number profiles at the hot and cold walls (from top to down) in time at $Ra = 10^6$.

Table 1. Comparison of $Nu_m$, $Nu_{\max}$, $Nu_{\min}$, $u_{\max}$ and $v_{\max.}$ Data with the literature.

| | Present work | de Vahl Davis (1983) | Barakos, Mitsoulis, and Assimacopoulos (1994) | Wakashima and Saitoh (2004) | Fusegi, Hyun, and Kuwahara (1991) |
|---|---|---|---|---|---|
| $Ra = 10^3$ | | | | | |
| $Nu_m$ | 1.1192 | 1.116 | 1.114 | – | 1.104 |
| $Nu_{\max}(y/L)$ | 1.5109(0.0875) | 1.501(0.087) | 1.581(0.099) | – | 1.420(0.083) |
| $Nu_{\min}(y/L)$ | 0.689(1.000) | 0.694(1.000) | 0.67(0.994) | – | 0.764(1.000) |
| $u_{\max}(y/L)$ | 3.6662(0.8125) | 3.634(0.813) | 4.0768(0.806) | – | 3.5172(0.833) |
| $v_{\max}(x/L)$ | 3.7203(0.175) | 3.679(0.179) | 4.1301(0.181) | – | 3.4906(0.200) |
| $Ra = 10^4$ | | | | | |
| $Nu_m$ | 2.2566 | 2.234 | 2.245 | 2.0676 | 2.302 |
| $Nu_{\max}(y/L)$ | 3.5432(0.1375) | 3.545(0.149) | 3.539(0.143) | – | 3.652(0.623) |
| $Nu_{\min}(y/L)$ | 0.5844(1.000) | 0.592(1.000) | 0.583(9.994) | – | 0.611(1.000) |
| $u_{\max}(y/L)$ | 16.2066(0.8250) | 16.182(0.823) | 16.2625(9.818) | 16.7259(0.8250) | 16.9366(0.817) |
| $v_{\max}(x/L)$ | 19.8964(0.1125) | 19.509(0.120) | 19.7172(0.119) | 18.6892(0.1125) | 18.9588(0.117) |
| $Ra = 10^5$ | | | | | |
| $Nu_m$ | 4.5260 | 4.51 | 4.51 | 4.3907 | 4.646 |
| $Nu_{\max}(y/L)$ | 7.5841(0.0875) | 7.761(0.085) | 7.636(0.085) | – | 7.795(0.083) |
| $Nu_{\min}(y/L)$ | 0.7429(1.000) | 0.736(1.000) | 0.733(0.999) | – | 0.787(1.000) |
| $u_{\max}(y/L)$ | 34.7451(0.8625) | 34.81(0.855) | 35.1725(0.859) | 37.7838(0.8500) | 39.1694(0.855) |
| $v_{\max}(x/L)$ | 70.4475(0.0625) | 68.22(0.066) | 69.7462(0.066) | 65.2823(0.0625) | 65.8152(0.065) |
| $Ra = 10^6$ | | | | | |
| $Nu_m$ | 8.6123 | 8.798 | 8.806 | 8.8681 | 9.012 |
| $Nu_{\max}(y/L)$ | 16.1274(0.0375) | 18.076(0.0456) | 17.442(0.0368) | – | 17.670(0.0379) |
| $Nu_{\min}(y/L)$ | 1.0823(1.000) | 1.005(1.000) | 1.001(0.999) | – | 1.257(1.000) |
| $u_{\max}(y/L)$ | 63.0338(0.8625) | 65.33(0.851) | 64.8814(0.859) | 68.2939(0.8500) | 70.7797(0.856) |
| $v_{\max}(x/L)$ | 229.7988(0.0375) | 216.75(0.0387) | 220.7651(0.039) | 219.5855(0.0375) | 218.2373(0.033) |

oscillations but similar to the previous case, it is damped out and then it reaches a steady state.

Furthermore, time evolution of streamlines, temperature profiles and $Nu$ profiles at hot and cold walls are provided in Figures 5–8. In Figure 5, snapshots are taken at equal time intervals. It is observed that streamlines, temperature profiles and $Nu$ profiles are slowly reaching a steady state. This is expected according to Figure 4. On the other hand, in Figure 6, first snapshots are taken at a time between initial state and first peak of $Nu_m$ in Figure 4. A second snapshot is taken at the first peak of $Nu_m$ in Figure 4, the third snapshot is taken at the local minima after the peak of $Nu_m$ in Figure 4 and the fourth snapshot is taken at a time where $Nu_m$ in Figure 4 is steady. The effect of peak can be observed in streamlines, temperature and $Nu$ profiles and all of these oscillate before reaching a steady state. Moreover, in Figure 7, local maxima, local minima and a point where $Nu_m$ is steady are selected to be the points where five snapshots are taken. Similar to the previous case, oscillations of streamlines, temperature and $Nu$ profiles are more obvious in Figure 7. Furthermore, in Figure 8, oscillations become more frequent and significant.

### *5.2. Validation of the method*

Results obtained in this study are compared to the results available in the literature. In Table 1, mean Nusselt number ($Nu_m$), maximum Nusselt number ($Nu_{\max}$), minimum Nusselt number, ($Nu_{\min}$), maximum $u$ velocity ($u_{\max}$), maximum $v$ velocity ($v_{\max}$) for Rayleigh number interval $10^3-10^6$ are compared. Nusselt number values are calculated at the hot wall, $u$ velocity values are calculated at the half-width plane of the cavity and $v$ velocity values are calculated at the half-height plane of the cavity. Locations of maximum and minimum points in Table 1 are chosen to be the actual location of grid points. In other words, no interpolation is made to find the maximum and minimum points. Results show that original solution obtained in this study is in a very good agreement with available results in the literature.

## 6. Conclusion

Transient and laminar natural convection in a square cavity problem is analysed using ISPH method. Unlike the common practice seen in SPH literature, particles remained stationary in this study. This is achieved by employing a Eulerian form of governing equations instead of Lagrangian forms. As a consequence, density error accumulation and particle disordering are prevented. Since these are one of the most prominent causes of error in SPH computations, this approach is thought to be the upper limit for SPH computations. Furthermore, the effect of $Ra$ number is investigated and results are validated by available data in the literature. It is seen that results obtained by the approach presented in this study are in a very good agreement with the literature.

## References


Afshar, M., and G. Shobeyri. 2010. Efficient simulation of free surface flows with discrete least-squares meshless method using a priori error estimator. *International Journal of Computational Fluid Dynamics* 24, no. 9: 349–67.

Barakos, G., E. Mitsoulis, and D. Assimacopoulos. 1994. Natural convection flow in a square cavity revisited: Laminar and turbulent models with wall functions. *International Journal for Numerical Methods in Fluids* 18, no. 7: 695–719.

Chaniotis, A., D. Poulikakos, and P. Koumoutsakos. 2002. Remeshed smoothed particle hydrodynamics for the simulation of viscous and heat conducting flows. *Journal of Computational Physics* 182, no. 1: 67–90.

Chen, J., and J. Beraun. 2000. A generalized smoothed particle hydrodynamics method for nonlinear dynamic problems. *Computer Methods in Applied Mechanics and Engineering* 190, no. 1: 225–39.

Ciarlet, P. 1978. *The finite element method for elliptic problems*. Vol. 4. Amsterdam: North Holland.

Cleary, P., and J. Monaghan. 1999. Conduction modelling using smoothed particle hydrodynamics. *Journal of Computational Physics* 148, no. 1: 227–64.

Colin, F., R. Egli, and F. Lin. 2006. Computing a null divergence velocity field using smoothed particle hydrodynamics. *Journal of Computational Physics* 217, no. 2: 680–92.

Cummins, S., and M. Rudman. 1999. An SPH projection method. *Journal of Computational Physics* 152, no. 2: 584–607.

Davis, G. de Vahl. 1983. Natural convection of air in a square cavity: A bench mark numerical solution. *International Journal for Numerical Methods in Fluids* 3, no. 3: 249–64.

Dehnen, W., and H. Aly. 2012. Improving convergence in smoothed particle hydrodynamics simulations without pairing instability. *Monthly Notices of the Royal Astronomical Society* 425, no. 2: 1068–82.

Dilts, G. 1999. Moving-least-squares-particle hydrodynamics - I. Consistency and stability. *International Journal for Numerical Methods in Engineering* 44, no. 8: 1115–55.

Ellero, M., M. Serrano, and P. Espanol. 2007. Incompressible smoothed particle hydrodynamics. *Journal of Computational Physics* 226, no. 2: 1731–52.

Fusegi, T., J. Hyun, and K. Kuwahara. 1991. Three-dimensional simulations of natural convection in a sidewall-heated cube. *International Journal for Numerical Methods in Fluids* 13, no. 7: 857–67.

Giangi, M., and F. Stella. 1999. Analysis of natural convection during solidification of a pure metal. *International Journal of Computational Fluid Dynamics* 11, no. 3–4: 341–9.

Gingold, R., and J. Monaghan. 1977. Smoothed particle hydrodynamics-theory and application to non-spherical stars. *Monthly Notices of the Royal Astronomical Society* 181: 375–89.

Gomez-Gesteira, M., B.D. Rogers, A.J.C. Crespo, R.A. Dalrymple, M. Narayanaswamy, and J.M. Dominguez. 2012. SPHysics-development of a free-surface fluid solver - part 1: Theory and formulations. *Computers & Geosciences* 48: 289–99.

Hosseini, S., M. Manzari, and S. Hannani. 2007. A fully explicit three-step SPH algorithm for simulation of non-Newtonian fluid flow. *International Journal of Numerical Methods for Heat & Fluid Flow* 17, no. 7: 715–35.

Hu, X., and N. Adams. 2007. An incompressible multi-phase SPH method. *Journal of Computational Physics* 227, no. 1: 264–78.

Ilicak, M., A. Ecder, and E. Turan. 2007. Operator splitting techniques for the numerical analysis of natural convection heat transfer. *Computer Mathematics* 84, no. 6: 783–93.

Kohno, H., and T. Tanahashi. 2005. Numerical analysis of thermal melt flow and melt/solid interface shapes in the floating zone method. *International Journal of Computational Fluid Dynamics* 19, no. 3: 243–51.

Kuznetsov, G., and L. Sitnikova. 2004. Numerical analysis of the influence of natural convection on the process of condensation of atmospheric pollutant compounds on the surface of near-ground plants. *Journal of Engineering Physics and Thermophysics* 77, no. 5: 939–46.

Lappa, M. 2004. An "attachment kinetics-based" level-set method for macromolecular crystallization under buoyancy-driven convective effects. *International Journal of Computational Fluid Dynamics* 18, no. 7: 615–21.

Liu, G., and M. Liu. 2003. *Smoothed particle hydrodynamics: A meshfree particle method*. Singapore: World Scientific.

Liu, M., and G. Liu. 2010. Smoothed particle hydrodynamics (SPH): An overview and recent developments. *Archives of Computational Methods in Engineering* 17, no. 1: 25–76.

Lucy, L. 1977. A numerical approach to the testing of the fission hypothesis. *The Astronomical Journal* 82: 1013–24.

Monaghan, J.. 1994. Simulating free surface flows with SPH. *Journal of Computational Physics* 110, no. 2: 399–406.

Monaghan, J. 2000. SPH without a tensile instability. *Journal of Computational Physics* 159, no. 2: 290–311.

Morris, J., P. Fox, and Y. Zhu. 1997. Modeling low Reynolds number incompressible flows using SPH. *Journal of Computational Physics* 136, no. 1: 214–26.

Nelson, R., B. Butler, and D. Weise. 2012. Entrainment regimes and flame characteristics of wildland fires. *International Journal of Wildland Fire* 21, no. 2: 127–40.

Oden, J., and K. Vemaganti. 2000. Estimation of local modeling error and goal-oriented adaptive modeling of heterogeneous materials I. Error estimates and adaptive algorithms. *Journal of Computational Physics* 164, no. 1: 22–47.

Oger, G., M. Doring, B. Alessandrini, and P. Ferrant. 2007. An improved SPH method: Towards higher order convergence. *Journal of Computational Physics* 225 no. 2: 1472–92.

Pozorski, J., and A. Wawrenczuk. 2002. SPH computation of incompressible viscous flows. *Journal of Theoretical and Applied Mechanics* 40: 917–37.

Prudhomme, S., and J. Oden. 1999. A posteriori error estimation and error control for finite element approximations of the time-dependent Navier–Stokes equations. *Finite Elements in Analysis and Design* 33, no. 4: 247–62.

Prudhomme, S., and J. Oden. 2002. Computable error estimators and adaptive techniques for fluid flow problems. *Lecture Notes in Computational Science and Engineering* 25: 207–68.

Randles, P., and L. Libersky. 1996. Smoothed particle hydrodynamics: Some recent improvements and applications. *Computer Methods in Applied Mechanics and Engineering* 139, no. 1: 375–408.

Ren, J., J. Ouyang, B. Yang, T. Jiang, and H. Mai. 2011. Simulation of container filling process with two inlets by improved smoothed particle hydrodynamics (SPH) method. *International Journal of Computational Fluid Dynamics* 25, no. 7: 365–86.

Roache, P.. 1997. Quantification of uncertainty in computational fluid dynamic. *Annual Review of Fluid Mechanics* 29: 123–60.

Schoenberg, I. 1946. Contributions to the problem of approximation of equidistant data by analytic functions. *Quarterly of Applied Mathematics* 4, no. Part A: 45–99.

Shao, J., H.Q. Li, G.R. Liu, and M.B. Liu. 2012. An improved SPH method for modeling liquid sloshing dynamics. *Computers & Structures* 100: 18–26.

Shao, S., and E. Lo. 2003. Incompressible SPH method for simulating Newtonian and non-Newtonian flows with a free surface. *Advances in Water Resources* 26, no. 7: 787–800.

Szewc, K., J. Pozorski, and J. Minier. 2012. Analysis of the incompressibility constraint in the smoothed particle hydrodynamics method. *International Journal for Numerical Methods in Engineering* 92, no. 4: 343–69.

Szewc, K., J. Pozorski, and A. Tanière. 2011. Modeling of natural convection with smoothed particle hydrodynamics: Non-Boussinesq formulation. *International Journal of Heat and Mass Transfer* 54, no. 23–24: 4807–16.

Teamah, M., M. Dawood, and W. El-Maghlany. 2011. Double diffusive natural convection in a square cavity with segmental heat source. *European Journal of Scientific Research* 54, no. 2: 287–301.

van der Vorst, H.A. 1992. BI-CGSTAB: A fast and smoothly converging variant of BI-CG for the solution of nonsymmetric linear systems. *SIAM Journal on Scientific and Statistical Computing* 13, no. 2: 631–44.

Wakashima, S., and T. Saitoh. 2004. Benchmark solutions for natural convection in a cubic cavity using the high-order time-space method. *International Journal of Heat and Mass Transfer* 47, no. 4: 853–64.

Xu, R., P. Stansby, and D. Laurence. 2009. Accuracy and stability in incompressible SPH (ISPH) based on the projection method and a new approach. *Journal of Computational Physics* 228, no. 18: 6703–25.